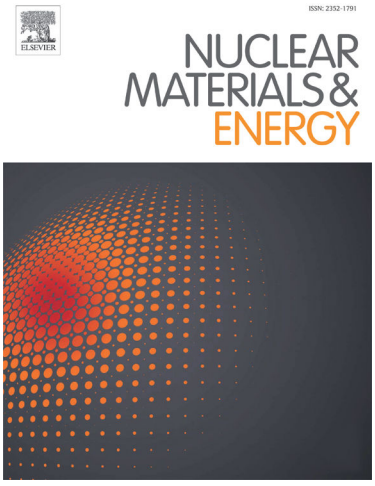

Locations of cleavage initiation sites in miniaturized C(T) specimens and their relation to mechanical field quantities

Timo Metzler, Ermile Gaganidze, Jarir Aktaa

PII: S2352-1791(26)00042-6
DOI: https://doi.org/10.1016/j.nme.2026.102099
Reference: NME 102099

To appear in: *Nuclear Materials and Energy*

Received Date: 1 May 2025
Revised Date: 27 October 2025
Accepted Date: 11 March 2026

Please cite this article as: T. Metzler, E. Gaganidze, J. Aktaa, Locations of cleavage initiation sites in miniaturized C(T) specimens and their relation to mechanical field quantities, *Nuclear Materials and Energy* (2026), doi: https://doi.org/10.1016/j.nme.2026.102099

Locations of cleavage initiation sites in miniaturized C(T) specimens and their relation to mechanical field quantities

Timo Metzler*, Ermile Gaganidze, Jarir Aktaa

Karlsruhe Institute of Technology (KIT), Hermann-von-Helmholtz-Platz 1, 76344 Eggenstein-Leopoldshafen, Germany

Abstract

The miniaturized C(T) specimen is a promising geometry to be used in future surveillance programs for the long-term operation of second-generation nuclear reactors. In multiple studies, the geometry was shown to provide Master Curve reference temperature values comparable to standard-sized C(T) specimens. International testing standards such as ASTM E1921 additionally require cleavage fracture to occur under high constraint conditions. Due to its reduced thickness, constraint loss is observed in the miniaturized C(T) specimen at high crack tip loads. In order to validate the miniaturized C(T) geometry, it must be ensured that cleavage initiation still occurs under similar conditions as with standard-sized C(T) specimens.

In this study, the locations of cleavage initiation sites in miniaturized C(T) specimens of SA-508 Cl.3 reactor pressure vessel steel are determined by means of scanning electron microscopy. Applying finite-element-analysis, the mechanical fields in front of the crack tip, namely the maximum principal stress, stress triaxiality and equivalent plastic strain, are obtained. By relating the locations of the initiation sites to the mechanical field quantities, the conditions for cleavage fracture are deduced. Particular attention is paid to the stress triaxiality, which is used as a measure of crack tip constraint. The mechanical fields of miniaturized specimens are compared to standard-sized geometries to evaluate similarities and differences in the fracture behavior based on the load level. It is shown that cleavage fracture initiation in miniaturized specimens remains located within a region of high crack tip constraint, even when significant macroscopic plastic deformation occurs prior to failure. Consequently, the conditions for cleavage initiation are found to be similar in miniaturized and standard-sized C(T) geometries.

Keywords

Fracture mechanics; Fractography; Cleavage initiation sites; Small specimen testing; Master Curve

* Corresponding author.

E-mail address: timo.metzler@kit.edu (T. Metzler).

1. Introduction

Small specimen testing has become essential for extending the service life of Generation II nuclear reactors, as the supply of irradiated standard-sized specimens from surveillance programs is highly limited [1,2]. To address this issue, plans are in place to increase the number of available specimens by extracting sub-sized specimens from the broken halves of standard-sized Charpy impact and fracture mechanics specimens previously tested in monitoring programs. From a manufacturing standpoint, a single broken Charpy specimen can yield up to eight miniaturized compact tension (MCT) specimens with a thickness of 4 mm [3]. The MCT has become the predominant geometry for small-specimen fracture toughness testing due to its balance between mechanical validity, microstructural representativeness and experimental feasibility. Small specimens offer additional advantages, including a lower active mass, which facilitates handling, and a smaller volume, allowing more specimens to be irradiated simultaneously in a reactor.

However, small specimen testing also presents challenges due to size-dependent effects. With decreasing specimen size, an increase in apparent fracture toughness is observed due to the stress state in front of the crack tip transitioning from plane-strain to plane stress [4]. At a certain point, fracture toughness measurements no longer represent the intrinsic fracture toughness of the material. Furthermore, as the characteristic microstructural size, such as the grain size or distance between inclusions, is approached, the fracture process is no longer statistically representative. On the practical side, fatigue pre-cracking procedures, accurate crack length determination as well as load control become increasingly difficult with decreasing specimen size. Through these mechanical, microstructural and practical limitations, a lower bound on specimen size for fracture toughness evaluation is imposed. Moreover, weakest link statistics often necessitate an increased number of small specimens to obtain valid fracture toughness results under internationally recognized testing standards such as ASTM E1921 [5]. Consequently, the accurate quantification and prediction of these size-dependent effects is crucial to minimizing the number of specimens required for fracture toughness evaluation.

This research is conducted as part of the FRACTESUS project [6,7], which aims to demonstrate and validate the use of small specimens for evaluating the fracture toughness of RPV steels in the ductile-to-brittle transition (DBT) region. Within the project, it has been shown that the reference temperature T_0 obtained from MCT specimens is comparable to that determined from standard-sized specimens [3]. To further validate the MCT geometry, it is necessary to demonstrate that the conditions for cleavage fracture in miniaturized and standard-sized geometries are similar. Cleavage fracture is typically initiated at a single location ahead of the fatigue crack at a specific position along the crack front [8]. The cleavage initiation sites on the fracture surfaces of MCT specimens are identified using scanning electron microscopy (SEM) and compared to those previously observed on standard-sized specimens. Additionally, the initiation sites are characterized based on the type of initiator. The mechanical fields in the vicinity the crack front, such as crack opening stress and stress triaxiality, are determined through finite-element (FE) simulation and compared at various levels of crack tip loading to assess constraint differences between the geometries. A cohesive zone model is employed to simulate material separation and crack extension during loading. Finally, the mechanical fields are correlated with the initiation site locations to characterize the conditions for cleavage fracture. This allows for a comparison of the fracture-mechanical behavior between miniaturized and standard-sized specimens, facilitating the assessment of the limitations of the MCT geometry.

2. Material and methodology

For the experimental and numerical investigations carried out in this work, the low-alloy RPV steel SA-508 Class 3 is used in the unirradiated condition. Applications of the material include RPVs, steam generators and pressurizers. The material block used for to the fabrication of tensile and fracture mechanics specimens was cut from the replacement closure head of the RPV of the José Cabrera power plant in Spain. The base metal was produced using electric furnace processing, followed by quenching to achieve a fine-grained microstructure. In Table 1, the chemical composition of the steel is listed.

Table 1. Chemical composition of the testing material SA-508 Cl.3 (in wt%).

C	Si	P	S	Cr	Mn	Ni	Cu	Mo	Fe
0.19	0.22	0.008	0.001	0.15	1.36	0.93	0.03	0.52	Balance

Fracture mechanics testing using MCT specimens was performed in [9-11] between -80 and -45°C and K_{Jc} values were determined according the ASTM E1921 standard. The specimens were loaded until failure and the critical J-integral at fracture J_{c} was calculated for each test from the force-displacement record. The J_{c} values were transformed into K_{Jc} following

$$K_{\mathrm{Jc}} = \sqrt{\frac{EJ_{\mathrm{c}}}{(1-\nu)^2}}, \tag{1}$$

where E is the elastic modulus and ν is Poisson's ratio. By means of the size-correction formula in the standard, the K_{Jc} results were subsequently transformed into 1T-equivalent values $K_{\mathrm{Jc,1T}}$ and a reference temperature T_0 of -31.5°C was obtained. Fracture-mechanical tests on 0.5T CT specimens were previously performed by Brynk et al. [12] using the material SA-508 Cl.3, resulting in a reference temperature of -43.6°C. The 0.5T CT specimens were extracted from the same forging as the MCT specimens tested in [9-11], although from a different section in both the circumferential as well as the radial direction. Macroscopic material inhomogeneities were shown to be present in the forging due to a spatially varying cooling rate during quenching. The T_0 values determined from the standard-sized and miniaturized specimens can be expected to be influenced by these inhomogeneities. In Fig. 1, the respective $K_{\mathrm{Jc,1T}}$ results and Master Curves obtained from both CT geometries are shown. Due to the plasticity limit imposed in the ASTM E1921 standard, the MCT specimens were predominantly tested at lower temperatures as compared to the 0.5T CT specimens. As most of the experimental MCT dataset was obtained from the tests at -60°C, this temperature is used for the calibration of the material model for the numerical simulations in this work.

The elastic modulus of the material at -60°C is determined using the equation

$$E = 204 - T/16 \text{ GPa} \quad (T \text{ in °C}), \tag{2}$$

which is derived for ferritic steels in the ASTM E1921 standard. The yield strength σ_{YS}, ultimate tensile strength UTS and percentage reduction of area RA were obtained from tensile tests on smooth round bar specimens that were performed in [9]. The mechanical properties of the material at -60°C are listed in Table 2.

Table 2. Mechanical properties of SA-508 Cl.3 at -60°C.

T [°C]	E [GPa]	σ_{YS} [MPa]	UTS [MPa]	RA [%]
-60	207.75	465	638	67.25

The determination of the uniaxial true stress–true plastic strain curve (flow curve) to be used as input for the elasto-plastic simulations was also performed in [9]. Smooth round bar specimens with a diameter of 2 mm and a gauge length of 5 mm were tested at -60°C until fracture. During testing, the respective specimen's contour was captured by a camera system to track the evolution of the minimum diameter and curvature radius in the necking region. The Bridgman correction method [13] was then applied to convert the multiaxial (average) true stress into the uniaxial true stress used in the plastic material model. The resulting flow curve for SA-508 Cl.3 at -60°C is shown in Fig. 2 (a).

In addition to tests on smooth round bar specimens, tests on notched round bars and fracture-mechanical tests on MCT specimens were conducted in [9] to determine the parameters of a cohesive zone model for the simulation of crack extension. The experiments on MCT specimens have shown that at -60°C, a limited amount of stable crack extension occurs prior to unstable fracture. In this work, the experiments were re-evaluated to calibrate the triaxiality dependent cohesive strength following

$$\sigma_c = 485 \cdot h + 1022.7 \text{ MPa}, \tag{3}$$

where h is the stress triaxiality. The stress triaxiality is the ratio of the hydrostatic stress to the Von Mises equivalent stress and can be used as a measure for the constraint of plastic deformation near the crack tip. For the second cohesive zone parameter, the cohesive energy, which is defined as the area under the traction-separation curve, a value of 1.67 N/mm is used. The calibration of the cohesive zone parameters was conducted using a hybrid experimental-numerical approach developed by Mahler & Aktaa [14], which includes testing and simulation of notched round bar and fracture mechanics specimens. A triangular shape of the traction-separation-law (TSL), as shown in Fig. 2 (b), is employed for simulating the low-temperature fracture mechanics experiments. To ensure a high initial stiffness, the cohesive strength σ_c is reached at 0.1% of the critical separation δ_c.

The fractographic investigations are conducted by means of SEM on the MCT specimens tested in [9-11] for the determination of the reference temperature. Fig. 3 shows the specimen geometry, which follows the ASTM E1921 standard, except for a 1.5 mm increase in the distance between the pin holes and the front face to accommodate an existing clip gauge extensometer. To calculate the fracture toughness K_{Jc} from each test, the recorded front face displacement was converted into the displacement at the load line using the geometric relationships proposed by Landes [15].

2.1 Initiation site fractography

The fractographic investigations are performed on the broken halves of the MCT specimens tested between -80°C and -45°C to locate and characterize the cleavage initiation sites. The micrographs are captured with a ZEISS EVO10 SEM equipped with a tungsten filament, utilizing both secondary and backscattered electron detectors at an acceleration voltage of 20 kV. To remove dust and loose particles, the fracture surfaces underwent ultrasonic cleaning in isopropanol for two minutes.

Cleavage initiation sites can be identified when transgranular cleavage is the dominant fracture mode, which is observed in all tested MCT specimens. The approach developed by Chekhonin et al. [16] is applied to locate the initiation sites and classify them based on the type of initiator. Once an initiation site is identified, high-magnification micrographs are taken to reveal potential initiating particles. If a particle is suspected at the center of an initiation site, EDX point measurements are conducted to determine its composition. The initiation site locations are later correlated with numerical stress and triaxiality fields near the crack front to evaluate the constraint conditions at fracture.

In Fig. 4, the procedure for locating the cleavage initiation sites is illustrated using specimen MCT08, which was tested at -70°C. A low-magnification overview image of the fracture surface (a) clearly shows "chevron markings" radiating from a distinct area near the crack front. These markings, which are revealed by height differences, generally fade as they approach the initiation site. The magnification is then progressively increased (b) to trace the "river lines" on individual cleavage facets back to a single point or a grain boundary. In the case of specimen MCT08, the river lines converge at a single point. The same process is repeated for the other specimen half, as the mirrored image of the initiation site may reveal features not visible on the initial fracture surface.

The measurement error of the cleavage fracture initiation site locations is the uncertainty in the spatial position of the identified initiation sites relative to the actual physical origin of fracture. Imaging limitations and interpretation uncertainties are the main factors contributing to the total measurement error. The river patterns and chevron markings are merely qualitative indicators, so different SEM operators might identify different cleavage origins. Regions of micro-void coalescence, secondary cracking and mechanical damage due to specimen handling may obscure the initiation site. Furthermore, SEM calibration errors and misalignment may contribute to the measurement error. In total, an uncertainty in the determined initiation site locations of ± 25 µm is estimated.

The described approach is generally uncomplicated for specimens tested well below T_0 and failing at low K_{Jc} values, as their fracture surfaces predominantly consist of transgranular cleavage facets. However, specimens tested closer to T_0 exhibit a mix of cleavage facets and regions of micro-void coalescence (quasi-cleavage), causing significant variation in the local crack growth direction. Consequently, multiple potential initiation sites often appear in close proximity, making it challenging to identify the primary initiator. As a result, the initiation sites could not be determined for several specimens tested at -60°C. Tracing the river lines on the cleavage facets, it is revealed that, although most lines point toward a specific region, they do not converge at a distinct point or grain boundary that can be definitively identified as the initiator.

2.2 Numerical modeling

Numerical simulations of the fracture mechanics tests are performed to determine the mechanical fields near the crack front. The MCT specimen and standard-sized CT geometries (0.5T and 1T CT) are modeled as 3D quarter geometries, with the mesh of the MCT model shown in Fig. 5. Geometric Symmetries in the xy- and xz-planes are taken into account by introducing appropriate boundary conditions in order to improve numerical efficiency. Loading is introduced by the wedge-shaped pin shown in brown, which is assumed to be rigid. An initial crack length to width ratio of $a_0/W = 0.5$ is assumed in all simulations.

Located in the crack plane starting from the initial crack front at $x = 0$, the cohesive zone consists of a strip of zero-thickness cohesive elements. The nodes on the upper surface of the cohesive elements are connected to the corresponding nodes of the surrounding continuum elements, while the nodes on the lower surface are constrained by boundary conditions. Between the cohesive zone and the specimen backside, a conventional symmetry condition in y-direction is used. As the MCT tests at -60°C terminated with only a small amount of stable crack propagation prior to unstable fracture, the length of the cohesive zone in x-direction is set to 0.1 mm.

The MCT model consists of about 22300 linear hexahedral continuum elements with eight integration points. Additionally, 680 cohesive elements are used in the crack plane. For the standard-sized CT

models, a similar number of elements is used. The mesh is highly refined near the cohesive zone, with the continuum elements directly at the crack plane having a length of 1.5 µm in both the x- and y-directions. The small element length is required to capture the large stress and strain gradients in the vicinity of the crack tip and small increments of crack extension. Ten elements are used in thickness direction, which are tapered towards the specimen side surface to accurately simulate necking at the crack tip.

3. Results

In the first step, the initiation sites found on the fracture surfaces of the SA-508 Cl.3 MCT specimens are characterized based on the type of initiator and their location. The initiation site locations are compared to the locations reported by other authors on MCT, SEB and larger CT specimens. Then, the numerical stress and triaxiality fields in front of the crack tip for MCT, 0.5T and 1T CT specimens are compared at multiple load levels in order to identify constraint differences between the geometries. Subsequently, the mechanical field quantities determined for the MCT geometry are correlated to the spatial distribution of initiation sites to evaluate the conditions for cleavage fracture.

3.1 Initiation site characteristics

Brittle fracture initiation in ferritic steels has been observed or is generally assumed to occur at fractured precipitates, inclusions, or grain boundaries [16-19]. By tracing the river pattern on the cleavage facets to its origin, two distinct types of initiation sites can be identified. In one case, the river lines converge toward a single point from multiple directions, while in the other, they point toward a grain boundary from one facet, with the river lines of the surrounding facets looping around the grain boundary.

The first type, shown in Fig. 6 (a, b), corresponds to cleavage fracture initiated at particle inclusions. The fractured or de-bonded particles, typically too small to be visible in SEM micrographs, act as initiation points from which the crack propagates outward in all directions. As the initiation site is approached, the river lines leading to it generally become less distinct. The second type, grain boundary initiation, is illustrated in Fig. 6 (c, d). Here, micro-crack propagation begins along a grain boundary, preventing the identification of a single initiation point. Instead, the river lines on the surrounding cleavage facets form a closed loop around the grain boundary, which typically appears as a topographic step. It is believed that a micro-crack originating from a grain boundary will eventually return to the initiation site. Since the crack plane shifts with each grain, this results in the formation of a step at the initial grain boundary [16].

The type of initiator was determined for 16 MCT specimens, with nine initiation sites (56%) exhibiting characteristics of particle initiation and seven (44%) located at grain boundaries. The initiation sites of the remaining six MCT specimens could not be characterized due to poor fracture surface quality or ambiguous river patterns. Chekhonin et al. (2023) [16] conducted an extensive fractographic analysis on 41 broken MCT specimens of unirradiated A508 Cl.3 RPV base metal steel, identifying 32% of initiators as Mo-rich carbides, 23% as Al-rich inclusions, and 38% as grain boundary initiators. The discrepancy in the particle versus grain boundary initiation ratio might be a consequence of the statistical uncertainty inherent in the limited specimen population analyzed in this work. The following section presents the results of EDX spot measurements at the suspected location of initiating particles.

EDX spot measurements were carried out on both fracture surfaces of all MCT specimens showing particle initiation. First, one measurement of the matrix material close to each initiation site was taken as a reference. Subsequent measurements were taken at the suspected locations of the initiating particles with about 1 µm distance between the individual spots. The locations of the matrix and particle measurements on the fracture surface of specimen MCT08 are shown in Fig. 7. The particle is positioned at the point where the river lines of multiple cleavage facets converge.

In Fig. 8 (a), the EDX spectrum of specimen MCT08 at the initiation site is shown. Compared to the reference spectrum (b), increased concentrations of S and Mn are found, indicating the presence of an MnS inclusion. An exact determination of the size of the inclusion by means of EDX is difficult, as the

inclusion is smaller than the interaction volume of the electron beam. From the micrograph, the size can be approximated to be less than 0.5 µm. On the other fracture surface of specimen MCT08, a similar concentration of S and Mn is found at the location of the particle. From this it can be concluded that micro-crack nucleation occurred by brittle fracture of the inclusion. Except for specimen MCT08, no increased concentration of the non-metals C, N, O and S or any metals commonly found in inclusions, such as Al, Mn, Mo and Cr were found at any initiation site. This is likely due to the small size of the inclusions, which makes it challenging to precisely locate the particles using EDX spot measurements.

In Fig. 9 (a), the locations of the initiation sites along the thickness direction, starting from the mid-thickness of the MCT specimens, are plotted against the respective $K_{\mathrm{Jc,1T}}$ values. The $K_{\mathrm{Jc,1T}}$ values were obtained by means of the fracture-mechanical tests described in Chapter 2. All initiation sites are located less than 1 mm from the mid-thickness of the 4 mm thick specimens. Within this range, the distances show considerable scatter, with no apparent correlation to the testing temperature. These findings align with a study by Wallin et al. [8], who analyzed the initiation site locations on the fracture surfaces of MCT specimens of the Japanese RPV steel SFVQ1A tested within the DBT region, and a study conducted by Das et al. [16] on irradiated MCT specimens of four different RPV steels. The clustering of initiation sites near the mid-thickness is likely due to the loss of constraint near the side surfaces. To confirm that cleavage initiation occurs under high-constraint conditions, numerical simulations are needed to evaluate the stress and triaxiality fields along the crack front.

The distance of the initiation sites from the crack front is shown in Fig. 9**Error! Reference source not found.** (b). It is defined as the distance from the local tip of the ductile crack extension to the initiation site in crack growth direction. The median distance between the initiation sites and the crack front is 66.2 µm. Most initiation sites are located around this distance with measurements ranging from 27 to 83 µm. There are four outliers located further from the crack front with distances up to 221 µm. As with the distance from the mid-thickness, the distance from the crack front appears to be uncorrelated to the testing temperature, but the scatter is more pronounced at higher temperatures. A positive correlation of $R = 0.72$ between the distance of the initiation sites from the crack front and $K_{\mathrm{Jc,1T}}$ is found by means of linear regression, meaning that on average, the distance increases with increasing loading. The coefficients a and b of the regression line are shown in the diagram. A positive correlation is according to expectations, as the distance from the crack front to the point of maximum crack opening stress—the primary driver of cleavage fracture—increases with increasing K_{J}. A similar result was observed by Das et al. [16] in both irradiated and unirradiated MCT specimens tested in the DBT region, emphasizing the consistency of the fracture-mechanical behavior of this geometry.

Ando et al. [20] investigated the initiation site locations on the fracture surfaces of standard-sized SEB specimens made of SM41C carbon steel and CT specimens of high-strength NiCrMoV steel. The SEB specimens had a thickness of 30 mm, while CT specimens with thicknesses of 7.5, 12.5, and 25 mm were tested. The SEB specimens were tested at -70, -50 and -30°C, while the CT tests were performed at -20°C. Similar to the findings for MCT specimens in this study and those by Wallin et al. [9] and Das et al. [16], nearly all initiation sites in larger geometries were located near the mid-thickness. However, on average, the initiation sites in larger specimens were located slightly closer to the surface. This is assumed to be due to the higher constraint in large specimens, which is analyzed in the following through numerical simulations.

3.2 Mechanical fields in front of the crack tip

Numerical simulations with different sizes of CT specimens are carried out to evaluate differences in the crack opening stress, stress triaxiality and the size of the plastic zone in the vicinity of the crack front. The quarter FE-model shown in Fig. 5 is used to simulate the MCT specimen and scaled versions of the model are used to simulate 0.5T CT and 1T CT geometries. The simulations are carried out at -60°C using the flow curve shown in Fig. 2 (a) and the cohesive zone model with the TSL shown in Fig. 2 (b). As mentioned above, the crack opening stress σ_{yy} is considered the main driver of cleavage fracture in ferritic steels as it causes brittle particles like MnS inclusions to fracture, resulting in micro-cracks that act as stress concentrators. In Fig. 10, the distribution of σ_{yy} is shown for the MCT geometry

at a crack tip load of $K_J = 35$ MPa$\sqrt{\text{m}}$. The maximum σ_{yy} of 1741 MPa is observed in the crack plane close to the crack tip ($x = 0$) and in the mid-thickness of the geometry ($z = 0$). With increasing distance from the crack tip and the mid-thickness the crack opening stress is reduced.

In the following diagrams, x represents the distance from the initial crack tip toward the specimen backside at the mid-thickness, while $z/(B/2)$ denotes the normalized distance from the mid-thickness to the side surface, based on the total thickness of the respective geometry. The graphs along the z -direction are positioned at the x-coordinate corresponding to the maximum value of the respective field quantity in the mid-thickness. The mechanical field quantities are analyzed under a low crack tip load of $K_J = 35$ MPa$\sqrt{\text{m}}$ and a moderate crack tip load of $K_J = 70$ MPa$\sqrt{\text{m}}$ to assess the potential loss of constraint with increasing deformation.

In Fig. 11, the crack opening stress is compared for the MCT, 0.5T and 1T CT geometries. Along the x -direction in the mid-thickness, a similar σ_{yy} is observed for both load levels (Fig. 11 (a, b)), with a slight overall decrease as the specimen size increases. Regardless of specimen size, the peak stress is reached at the same distance from the initial crack tip, which increases with increasing load.

In thickness direction at a crack tip load of $K_J = 35$ MPa$\sqrt{\text{m}}$ (Fig. 11 (c)), the standard-sized geometries maintain the peak opening stress until reaching the side surface, where σ_{yy} drops off. A similar behavior is observed for the MCT geometry, however, the reduction in σ_{yy} begins closer to the mid-thickness, at approximately 75% of the distance toward the side surface. At 70 MPa$\sqrt{\text{m}}$ (Fig. 11 (d)), the differences between the geometries become more pronounced. While the crack opening stress near the mid-thickness remains similar, in the case of the MCT the drop-off occurs already at 40% of the distance toward the side surface. In contrast, the reduction begins at 70% for the 0.5T CT and at 80% for the 1T CT geometry. At the side surfaces, the constraint of plastic deformation is reduced due to the prevailing plane stress condition. The elastic strain energy is consumed by the plastic deformation, causing the observed reduction in σ_{yy}. Due to the smaller thickness of the MCT specimen, this edge effect is more pronounced as compared to the larger geometries.

The triaxiality describes the local stress state in the loaded geometries and is used here to assess the constraint on plastic deformation near the crack front. The plane strain condition, which indicates high constraint, is reached at a certain distance from the side surface and is characterized by a saturation of triaxiality at its maximum value.

At a stress intensity factor $K_J = 35$ MPa$\sqrt{\text{m}}$, the triaxiality in the crack growth direction is nearly the same for all sizes of CT specimens, as shown in Fig. 12 (a). For the standard-sized geometries, the peak triaxiality of 2.9 is maintained in thickness direction until approaching the side surfaces (Fig. 12 (b)). In the case of the MCT geometry, the plane strain condition is sustained for about half the specimen thickness, while the triaxiality is gradually decreased as the side surface is approached. Similar to the crack opening stress, the triaxiality in the MCT geometry diverges further from the standard-sized geometries as the loading increases. At $K_J = 70$ MPa$\sqrt{\text{m}}$, the overall triaxiality near the crack front is lower in the MCT as compared to the standard-sized geometries. In crack growth direction (Fig. 12 (b)), the peak triaxiality for the 0.5T CT and 1T CT geometries remains at 2.9, while it is reduced to 2.7 for the MCT. In the thickness direction (Fig. 12 (d)), the peak triaxiality for the 1T CT geometry is maintained up to 75% of the distance to the side surface, and up to 55% for the 0.5T CT. For the MCT, no saturation of triaxiality near the mid-thickness is observed, and the peak value of 2.7 is only reached at $z = 0$ mm.

The evolution of triaxiality in front of the crack tip shows that, under high crack tip loading, the constraint level in the MCT specimen decreases throughout the entire thickness, causing the plane strain condition to be lost. In contrast, the constraint level in the standard-sized geometries remains constant across most of the thickness and only decreases near the side surfaces. However, at $K_J = 70$ MPa$\sqrt{\text{m}}$, the 0.2 decrease in triaxiality at the mid-thickness of the MCT is moderate.

The extent of the plastic zone ahead of the crack tip can be estimated using Irwin's stress relaxation model [21], which, for an elastic-perfectly plastic material, yields

$$R_{\mathrm{p}} = \frac{1}{\pi}\left(\frac{K_{\mathrm{I}}}{\sigma^{*}_{\mathrm{YS}}}\right)^{2}. \tag{4}$$

In this equation, σ^{*}_{YS} represents the yield strength of the material for plane stress and is equal to $\frac{1}{1-2\nu}\sigma_{\mathrm{YS}}$ for plane strain. The calculated plastic zone sizes for both plane stress and plane strain, based on Irwin's model, are plotted against K_{J} at -60°C in Fig. 13. These curves are compared to the simulated plastic zone lengths, starting from the crack tip at the mid-thickness of the MCT, 0.5T, and 1T CT geometries. In the simulations, the criterion for the identification of the plastic zone is a minimum equivalent plastic strain of 10^{-4}.

At crack tip loads below 20 MPa$\sqrt{\mathrm{m}}$, the simulated plastic zone sizes of the respective geometries are approximately equal to the calculated R_{p} for plane strain. This, along with the analysis of crack opening stress and triaxiality near the crack tip, indicates that the MCT can be considered a high-constraint geometry at low load levels. At crack tip loads exceeding 20 MPa$\sqrt{\mathrm{m}}$, all simulated curves begin to deviate from Irwin's plane strain estimation, showing larger plastic zone sizes. While this deviation is similar for the 0.5T and 1T CT geometries, it is more pronounced in the MCT. At 40 MPa$\sqrt{\mathrm{m}}$, the plastic zone in the MCT is almost twice the size of that in the 1T CT. This is further confirmation that much of the plane strain condition in MCT specimens is lost at lower K_{J} values as compared to the standard-sized geometries. Since at -60°C the K_{Jc} measurement capacity of the MCT assumed in the ASTM E1921 standard is significantly higher than 40 MPa$\sqrt{\mathrm{m}}$, this indicates that the specified $K_{\mathrm{Jc,limit}}$ may not be conservative enough to ensure plane strain conditions at fracture. However, a reduction of the limit would drastically increase the number of censored fracture toughness test results from MCT specimens.

As the plastic zone continues to grow for the larger geometries beyond 40 MPa$\sqrt{\mathrm{m}}$, the MCT experiences a deceleration in plastic zone growth. This is because the plastic zone is no longer small relative to the MCT's dimensions, and the crack tip stress field is influenced by the compressive stresses around the specimen's backside. At 40 MPa$\sqrt{\mathrm{m}}$, the plastic zone size at mid-thickness for the MCT is 21% of the initial crack length, while it is 4% and 2% for the 0.5T and 1T CT specimens, respectively.

3.3 Relation of initiation sites and mechanical fields

Following Ritchie et al. [22], the condition for cleavage fracture is that the local maximum principal stress σ_1 ahead of a stress concentrator exceeds a critical value over a characteristic distance. This critical fracture stress is assumed to be insensitive to temperature. For each MCT test, the fracture stress is obtained by evaluating the local maximum principal stress at the specific initiation site under fracture load. Based on a total of 14 tests between -80 and -60°C, the median fracture stress is 1734 MPa with a standard deviation of 97 MPa.

To ensure that the $K_{\mathrm{Jc,1T}}$ results from MCT specimens are comparable to the values obtained from different specimen types and sizes, the fracture behavior should be sufficiently similar. This means that the cleavage initiation sites should be located within the high-constraint region near the crack front. With the exception of two tests, brittle fracture initiation occurred within the area where the triaxiality exceeds 2. The triaxialities at the respective initiation sites range from 1.7 to 2.54. Additionally, most initiation sites are located within 35 µm of the points on the ligament where the maxima of σ_1 and h are observed.

The median K_{Jc} from the MCT specimens tested at -60°C is about $100\ \mathrm{MPa}\sqrt{\mathrm{m}}$ with a standard deviation of $20\ \mathrm{MPa}\sqrt{\mathrm{m}}$. The simulation is evaluated at this load level and in Fig. 14, the simulated

crack opening stress and triaxiality along the crack growth direction in the mid thickness of the MCT geometry (Fig. 14 (a, b)) and along the thickness direction (Fig. 14 (c, d)) are shown. In each diagram, the range of initiation site locations that were found on the specimens tested at -60°C is highlighted in gray and the median x and z coordinates of the initiation site locations are marked by the dashed black lines.

In crack growth direction, the initiation sites are between 35 to 221 µm from the crack tip, with the median distance being 60 µm. This corresponds exactly to the location of the maximum of σ_1 and is about 23 µm from triaxiality peak. Aside from two outliers with initiation sites around 200 µm from the crack tip, all initiation sites are close to the maxima of σ_1 and h. In the z-direction, the initiation sites are within 750 µm of the mid thickness with a median distance of 459 µm. As shown in Fig. 14 (c) and (d), the initiation sites are located in the region where both the maximum principal stress and triaxiality are nearly saturated. The maximum triaxiality at this load level is about 2.4, which is 0.5 below the maximum triaxiality of 2.9 observed at low load levels and in standard-sized geometries.

By relating the initiation site locations to the mechanical fields in near the crack front, it is confirmed that cleavage initiation in MCT specimens is strongly correlated to conditions of high stress and high triaxiality. Based on these results, it can be concluded that the fracture behavior of the MCT geometry aligns with theoretical expectations.

4. Discussion

In [10], a valid reference temperature was obtained for the RPV steel SA-508 Cl.3 from 19 MCT specimens, with two fracture toughness results requiring censoring for exceeding the plasticity limit specified in the ASTM E1921 standard. This shows that it is possible to determine the reference temperature from MCT specimens without a large amount of censored test results, as long as the tests are performed sufficiently below T_0. To further verify the MCT geometry for use in surveillance programs, the mechanical behavior of the MCT specimens was assessed in this work by comparing the numerical stress, triaxiality and plastic strain fields in front of the crack tip with those obtained on 0.5T and 1T CT geometries at 30°C below T_0.

At a low crack tip load of 35 MPa$\sqrt{\text{m}}$, the behavior of the geometries is found to be similar, with nearly identical stress profiles and the plane strain condition present across at least half of the specimen thickness. Thereby, it is confirmed that the MCT is a high-constraint geometry as long as no large-scale plastic deformation occurs. However, a strong increase in the size of the plastic zone ahead of the crack tip and, consequently, an overall decrease in triaxiality is observed for the MCT at a moderate crack tip load of 70 MPa$\sqrt{\text{m}}$. Meanwhile, the mechanical behavior of the 0.5T and 1T geometries in thickness direction remains comparable to the 35 MPa$\sqrt{\text{m}}$ case. Still, the MCT is shown to maintain a high level of triaxiality and crack opening stress near the mid thickness. Based on the fractographic investigations of the specimens tested at -60°C, it is confirmed that fracture occurs within this region of high constraint, which makes up about one third of the total thickness at the median fracture load of 100 MPa$\sqrt{\text{m}}$. The median distance of the initiation sites to the mid-thickness is 23% of the specimen thickness, which aligns with the findings of Ando et al. [20] on large CT specimens. However, the identified loss of constraint near the side surfaces may lead to the deactivation of potential crack initiation sources (particles, grain boundaries) located outside the high constraint region in the MCT specimens. This may lead to an increase of the apparent fracture toughness. Consequently, the MCT geometry can be expected to not always provide conservative K_{Jc} test results. Nevertheless, the MCT is shown not to modify the fracture mechanism of the material.

The experimental and numerical results generated in this work support the view of the MCT geometry as a viable candidate for future surveillance programs. Cleavage fracture is initiated under high constraint conditions, which is an essential prerequisite of the Master Curve approach. The fracture-mechanical behavior of the geometry at temperatures sufficiently below T_0 was shown to be in line with theoretical expectations and is comparable to standard-sized geometries. Ultimately, the narrow range of optimal test temperatures, which is a result of the increased loss of constraint at temperatures close to T_0, remains the main deficiency of the geometry.

5. Conclusion

The locations of the cleavage initiation sites on the fracture surfaces of MCT specimens of SA-508 Cl.3 steel were determined. Simultaneously, the stress, triaxiality and plastic strain fields ahead of the crack front were calculated numerically and compared to the mechanical fields obtained from standard-sized CT models. The initiation site locations were then related to the mechanical fields in order to assess the fracture behavior of the MCT specimens. The findings are summarized as follows:

- The initiation sites of both MCT and standard-sized CT geometries are located around the mid-thickness of the specimens, ranging up to half the distance towards the side surfaces.
- At low crack tip loads, the mechanical behavior of the MCT is similar to the standard-sized geometries. However, as the fracture load is approached, significant loss of constraint near the side surfaces and a moderate reduction in triaxiality near the mid thickness is observed.
- At 30°C below the reference temperature, the initiation site locations of MCT specimens are aligned with the region of high maximum principal stress and high constraint, where saturation behavior of the triaxiality is observed. This indicates that the fracture behavior is according to theoretical expectations and comparable to standard-sized geometries.
- The present results support the use of the MCT geometry for future surveillance programs.

CRediT authorship contribution statement

T. Metzler: Conceptualization, Methodology, Software, Formal analysis, Investigation, Writing – original draft. **E. Gaganidze:** Methodology, Resources, Writing – review & editing, Supervision. **J. Aktaa:** Resources, Writing – review & editing, Supervision, Funding acquisition.

Acknowledgements

This project has received funding from the Euratom research and training programme 2020-2024 under grant agreement No. 900014. The views and opinions expressed herein do not necessarily reflect those of the European Commission.

References

[1] M. Scibetta, E. Lucon, E. van Walle, Optimum use of broken Charpy specimens from surveillance programs for the application of the master curve approach, Int. J. Fract. 116 (2002) 231–244, https://doi.org/10.1023/A:1020165900918.

[2] E. Lucon, M. Scibetta, R. Chaouadi, E. van Walle, S.W. Dean, Use of miniaturized compact tension specimens for fracture toughness measurements in the upper shelf regime, J. ASTM Int. 3 (2006) 1–16, https://doi.org/10.1520/JAI13235.

[3] M. Sánchez, S. Cicero, M. Kirk, E. Altstadt, W. Server, M. Yamamoto, Using mini-CT specimens for the fracture characterization of ferritic steels within the ductile to brittle transition range: A review, Metals 13-1 (2023) 176, https://doi.org/10.3390/met13010176.

[4] M. A. Sokolov, Development of mini-compact tension test method for determining fracture toughness master curves for reactor pressure vessel steels, ORNL/TM-2017/275, Oak Ridge National Laboratory (2017), https://doi.org/10.2172/1360080.

[5] ASTM International, Standard test method for determination of reference temperature, To, for ferritic steels in the transition range. E1921-21, ASTM International, West Conshohocken, PA (2021), https://doi.org/10.1520/E1921-21.

[6] S. Cicero, M. Lambrecht, H. Swan, P. Arffman, E. Altstadt, T. Petit, F. Obermeier, B. Arroyo, J. A. Álvarez, R. Lacalle, Fracture mechanics testing of irradiated RPV steels by means of sub-

sized specimens: FRACTESUS project, Procedia Struct. Integr. 28 (2020) 61–66, https://doi.org/10.1016/j.prostr.2020.10.008.

[7] FRACTESUS project, Fracture mechanics testing of irradiated RPV steels by means of sub-sized specimens, https://fractesus-h2020.eu/.

[8] K. Wallin, M. Yamamoto, U. Ehrnstén, Location of initiation sites in fracture toughness testing specimens: The effect of size and side grooves, in: Proceedings of the ASME 2016 Pressure Vessels and Piping Conference - Volume 1B: Codes and Standards, Vancouver, British Columbia, Canada, 2016, https://doi.org/PVP2016-63078.

[9] T. Metzler, E. Gaganidze, J. Aktaa, Numerical Prediction of Fracture Toughness of a Reactor Pressure Vessel Steel Based on Experiments Using Small Specimens, in: Proceedings of the ASME 2023 Pressure Vessels & Piping Conference - Volume 1: Codes & Standards, Atlanta, Georgia, USA, 2023, https://doi.org/10.1115/PVP2023-105918.

[10] F. Naziris, R. Hernandez Pascual, T. Metzler, E. Gaganidze, I. Uytdenhouwen, M. Kolluri, Master Curve Evaluation Using Miniature C(T) Specimens as Part of a Round Robin Program Within the FRACTESUS Project, in: Proceedings of the ASME 2023 Pressure Vessels & Piping Conference - Volume 1: Codes & Standards, Atlanta, Georgia, USA, 2023, https://doi.org/10.1115/PVP2023-107254.

[11] T. Metzler, E. Gaganidze, J. Aktaa, Prediction of fracture toughness of a reactor pressure vessel steel in the ductile-to-brittle transition region based on a probabilistic cohesive zone model approach, J. Nucl. Mater. 605 (2025), DOI 10.1016/j.jnucmat.2024.155556.

[12] T. Brynk, I. Uytdenhouwen, P. Arffman, E. Altstadt, R. Kopriva, F. Obermeier, M. Serrano, Fractesus Project: Final Selection of RPV Materials for Unirradiated and Irradiated Round Robins, in: Proceedings of the ASME 2022 Pressure Vessels & Piping Conference - Volume 1: Codes & Standards, Las Vegas, Nevada, USA, 2022, https://doi.org/10.1115/PVP2022-83871.

[13] P.W. Bridgman, Studies in Large Plastic Flow and Fracture: With Special Emphasis on the Effects of Hydrostatic Pressure, Hardvard University Press, Cambridge, MA and London, England, 1964, https://doi.org/10.4159/harvard.9780674731349.

[14] M. Mahler, J. Aktaa, Approach for Determining Fracture Mechanical Properties from Tests on Small Size Specimens at Room Temperature, Procedia Mater. Sci. 3 (2014) 434–439, https://doi.org/10.1016/j.mspro.2014.06.073.

[15] J.D. Landes, J calculation from front face displacement measurement on a compact specimen, Int. J. Frac. (1980) 183–186, https://doi.org/10.1007/BF00018249.

[16] P. Chekhonin, A. Das, F. Bergner, E. Altstadt, Microstructural characterization of brittle fracture initiation sites in reactor pressure vessel steels, Nucl. Mater. Energy 37 (2023) 101511, https://doi.org/10.1016/j.nme.2023.101511.

[17] D. A. Curry, J. F. Knott, Effect of microstructure on cleavage fracture toughness of quenched and tempered steels, Met. Sci. 13-6 (1979) 341–345, https://doi.org/10.1179/msc.1979.13.6.341.

[18] P. Bowen, S. G. Druce, J. F. Knott, Effects of microstructure on cleavage fracture in pressure vessel steel, Acta Metall. 34-6 (1986) 1121–1131, https://doi.org/10.1016/0001-6160(86)90222-1.

[19] S. Lee, S. Kim, B. Hwang, B. S. Lee, C. G. Lee, Effect of carbide distribution on the fracture toughness in the transition temperature region of an SA 508 steel, Acta Mater. 50-19 (2002) 4755–4762, https://doi.org/10.1016/S1359-6454(02)00313-0.

[20] K. Ando, K. Mogami, K. Tuji, Probabilistic aspects of cleavage crack initiation sites and fracture toughness, Fatigue Frac. Eng. Mater. Struct. 15 (1992) 1171-1184, https://doi.org/10.1111/j.1460-2695.1992.tb01255.x.

[21] G. R. Irwin, Plastic zone near a crack and fracture toughness, Proceedings of the 7th Sagamore Ordnance Materials Research Conference, Syracuse, New York, USA, 1960.

[22] R. O. Ritchie, J. F. Knott, J. R. Rice, On the relationship between critical tensile stress and fracture toughness in mild steel, J. Mech. Phys. Solids 21-6 (1973) 395–410, https://doi.org/10.1016/0022-5096(73)90008-2.

- Cleavage fracture initiation sites of MCT and standard-sized CT specimens are located around mid-thickness
- Significant loss of constraint near side surfaces of MCT specimens is observed as fracture load is approached
- Initiation site locations are aligned with region of high constraint where saturation of triaxiality is observed
- Fracture behavior of MCT specimens is comparable to standard-sized specimens

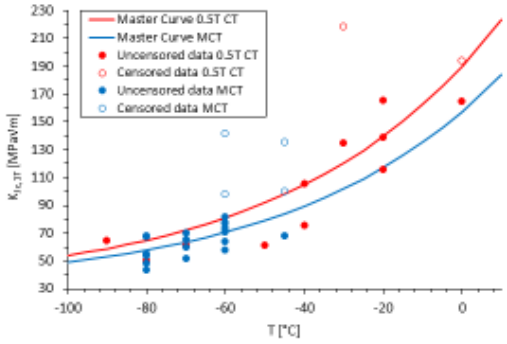

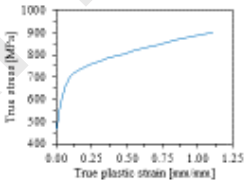

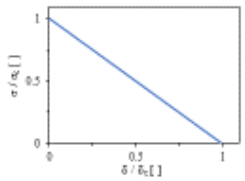

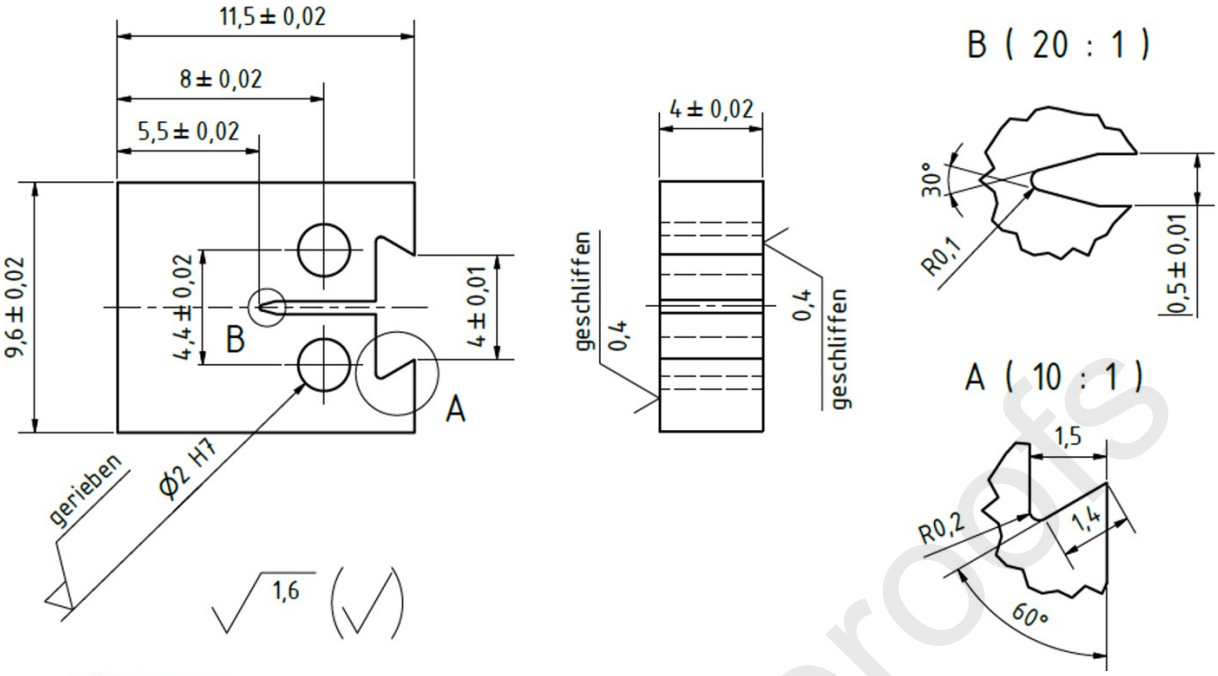

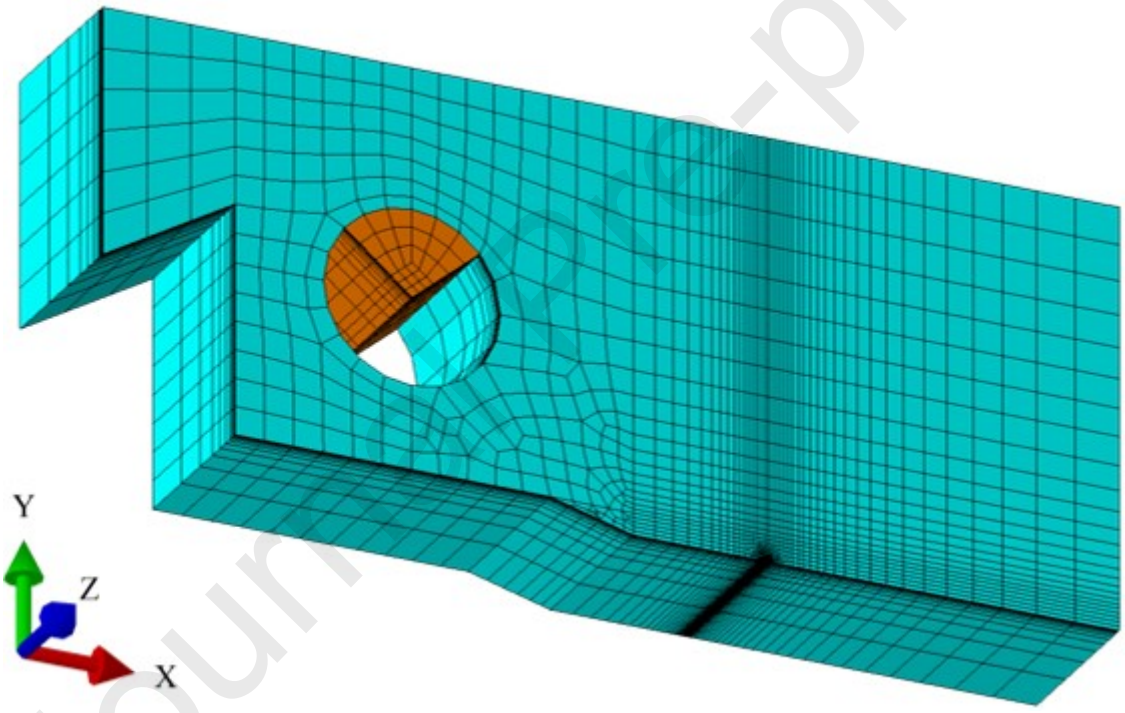

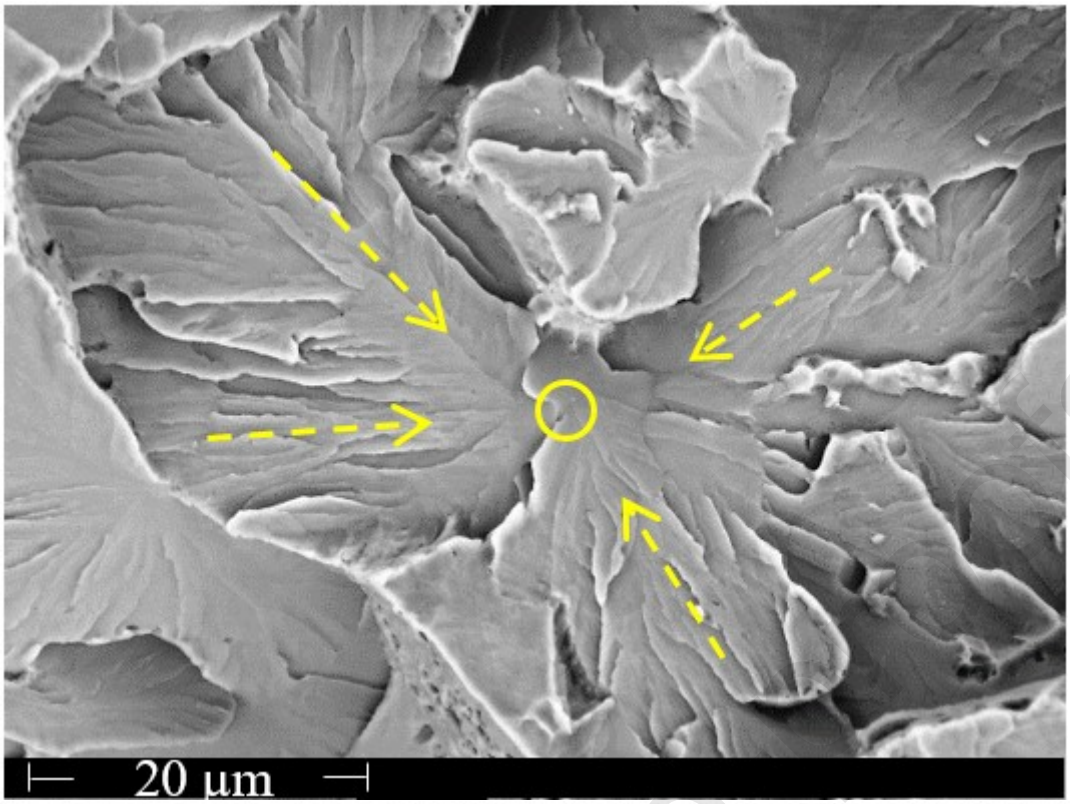
20 µm

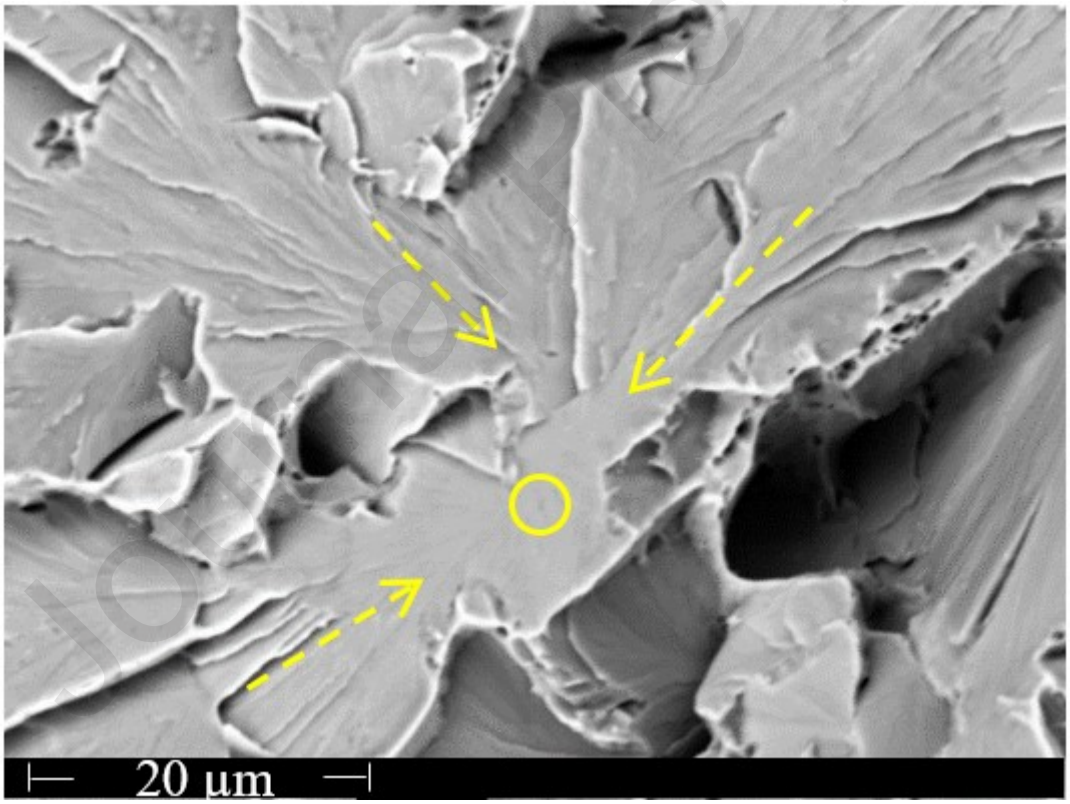
20 µm

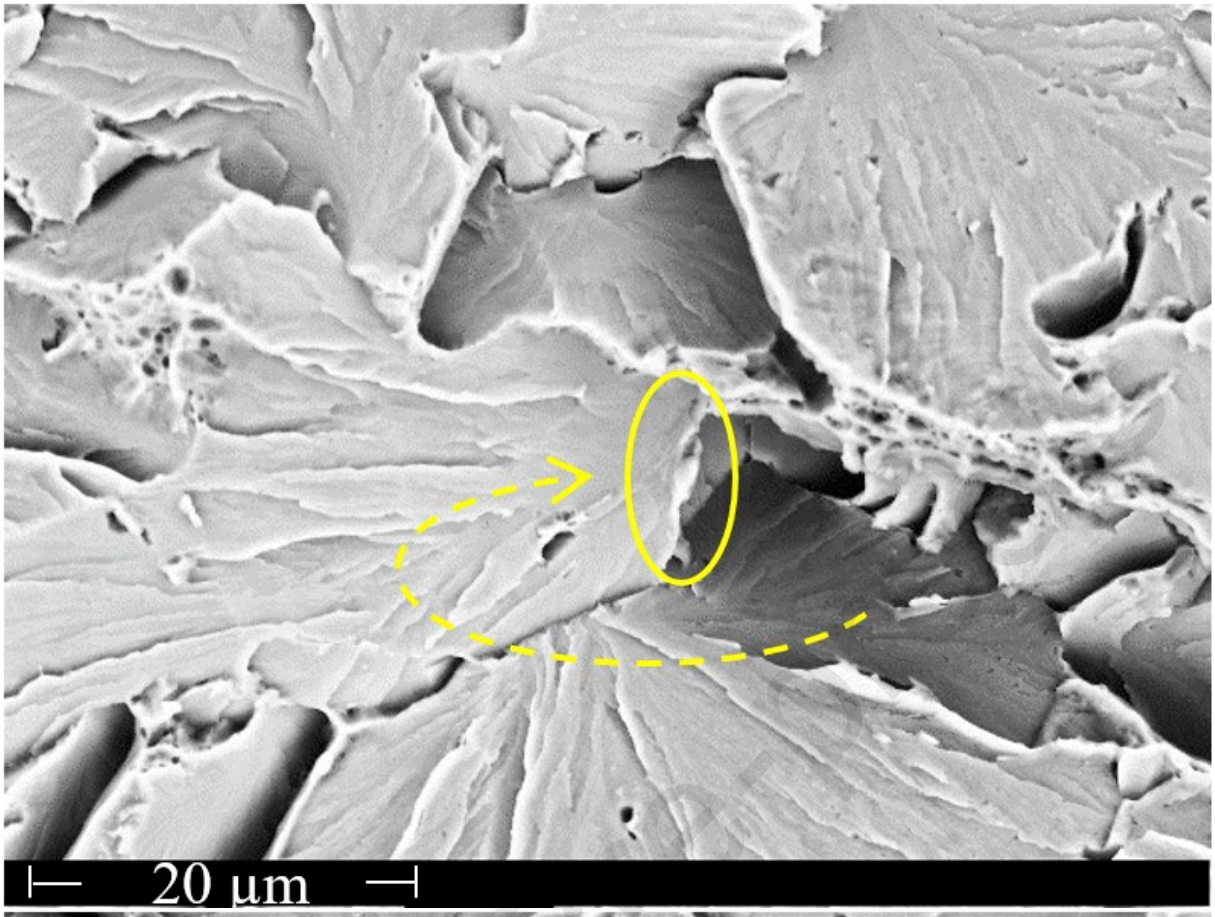
20 µm

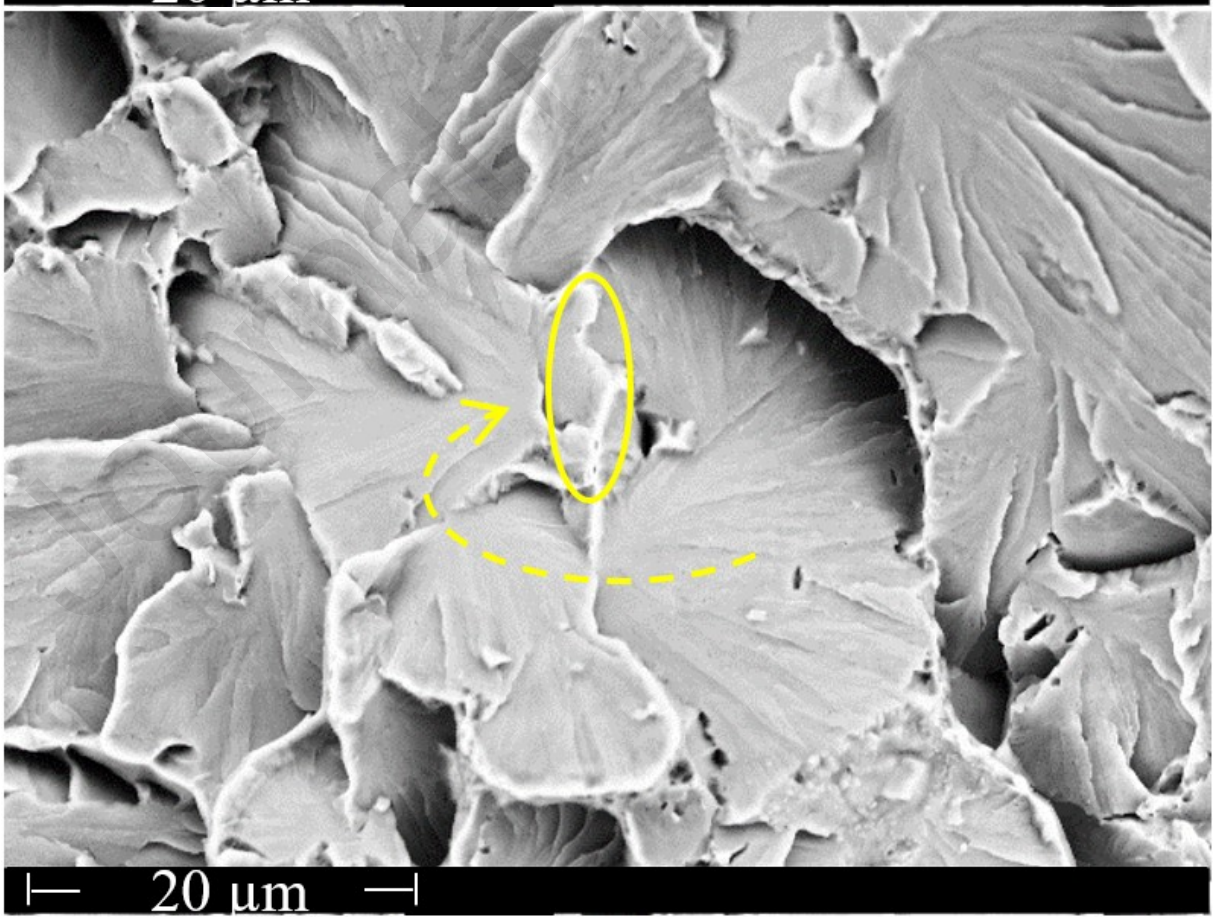
20 µm

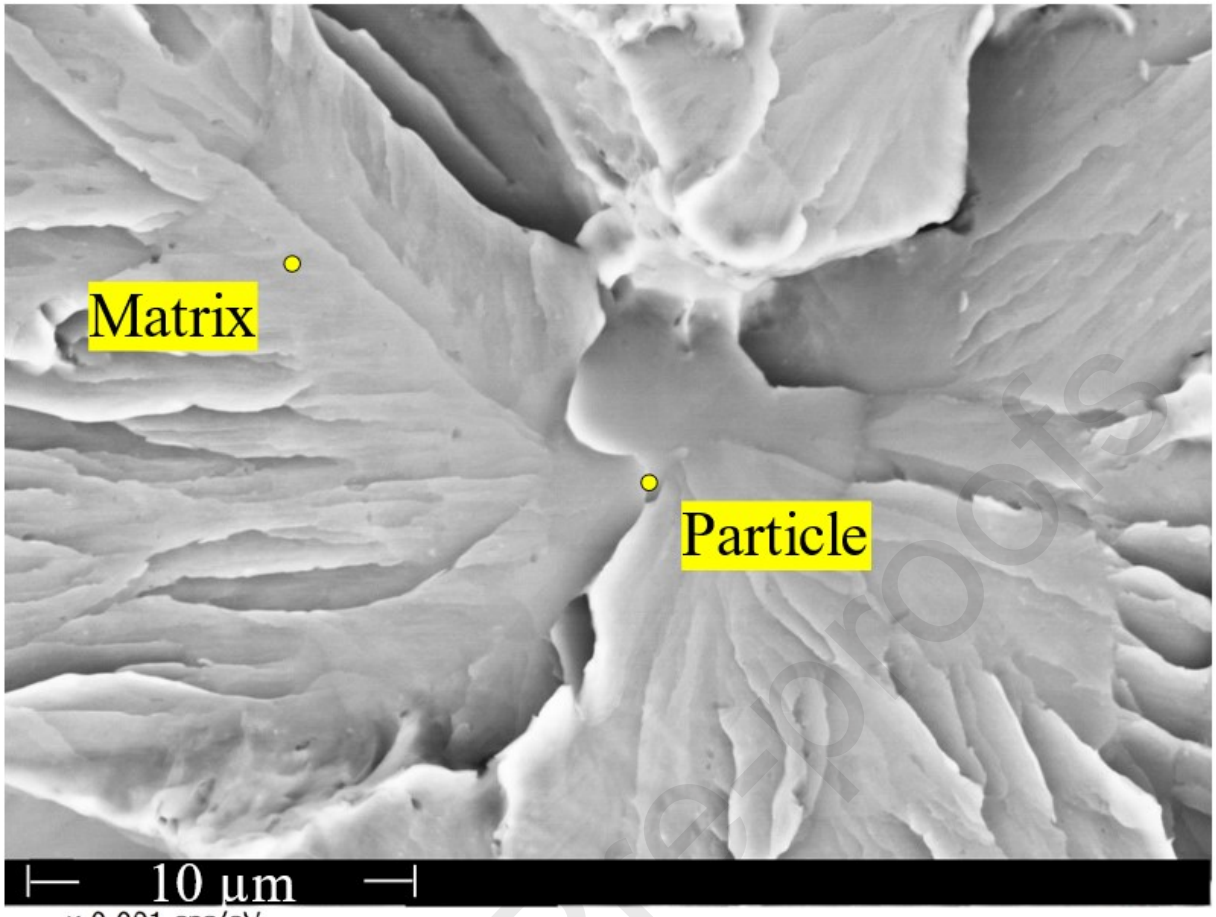

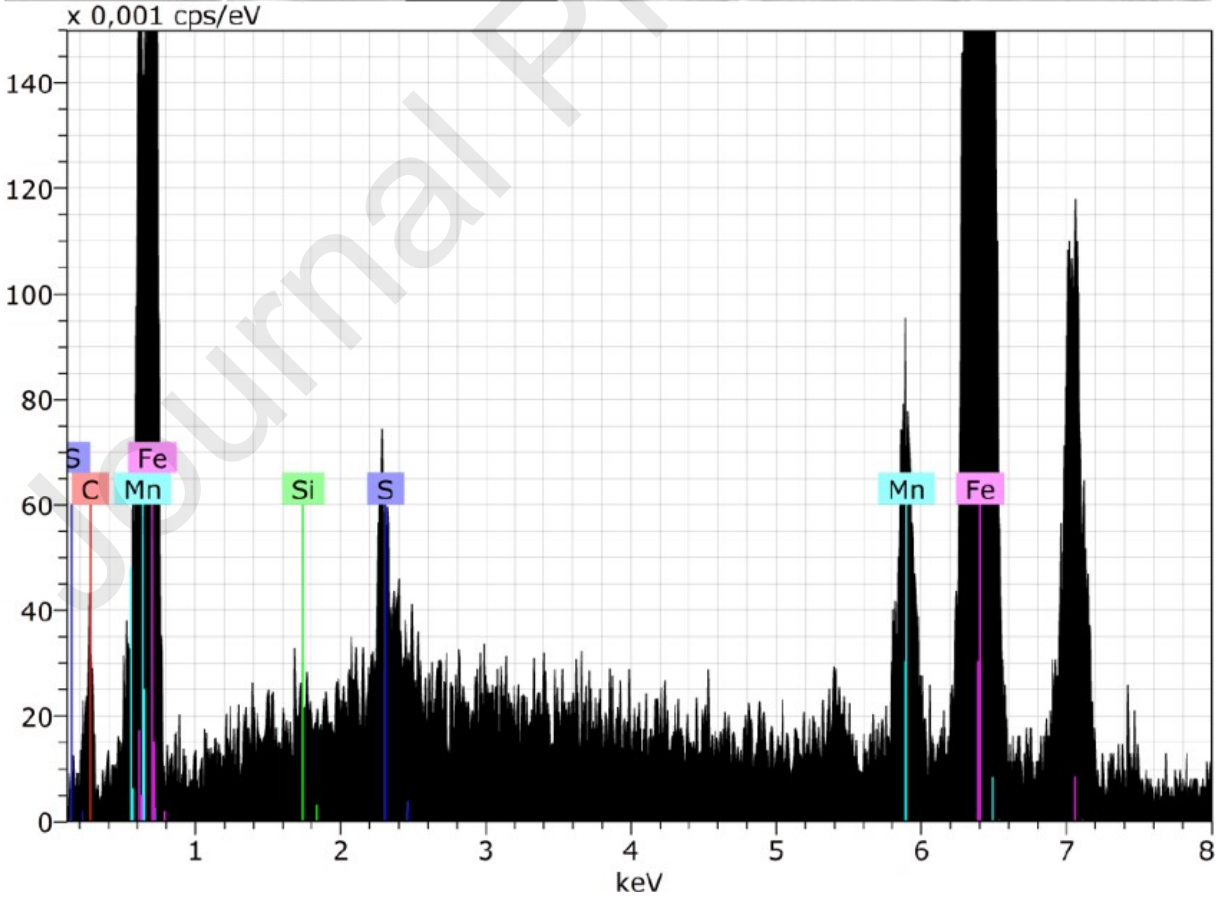

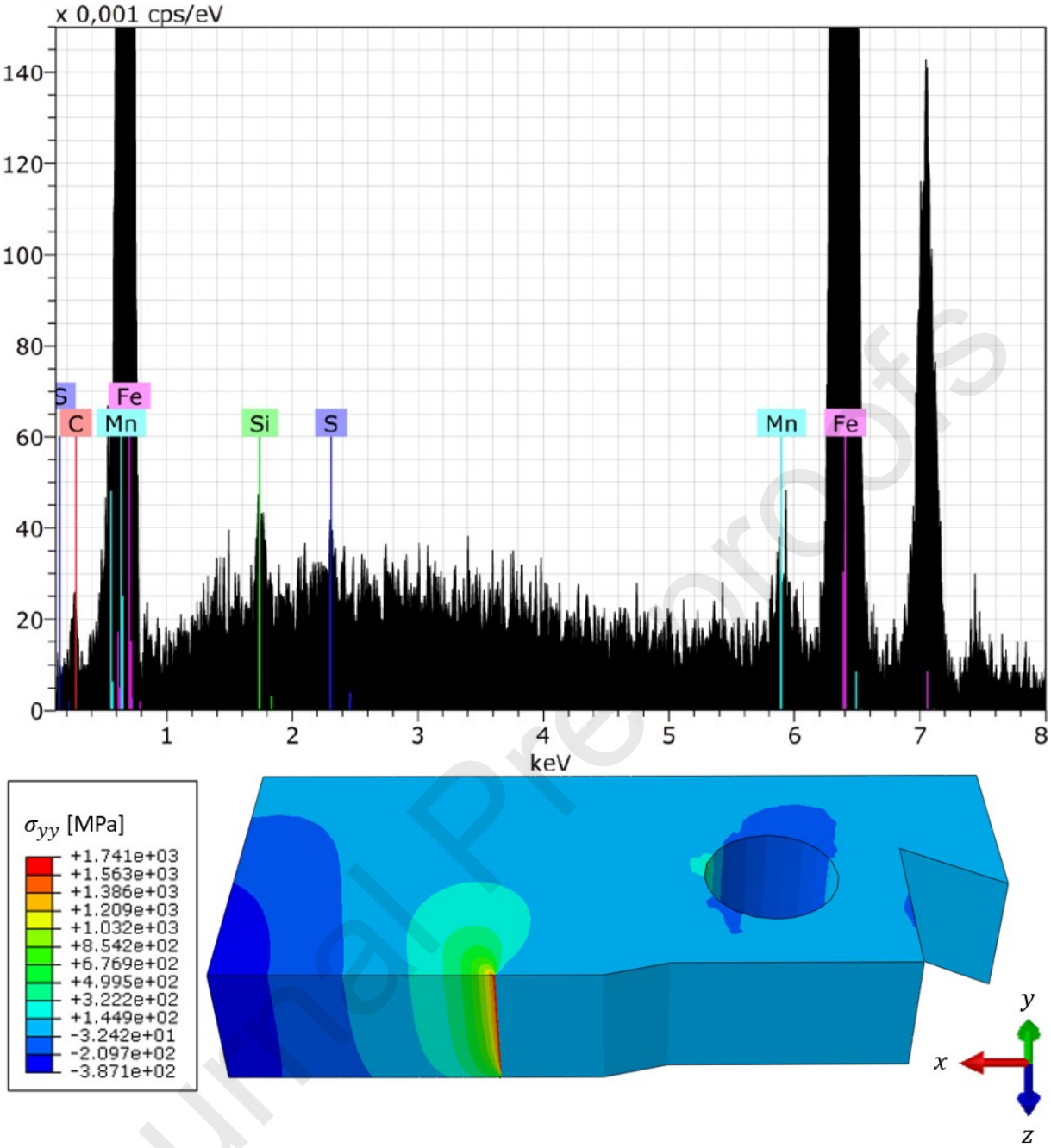

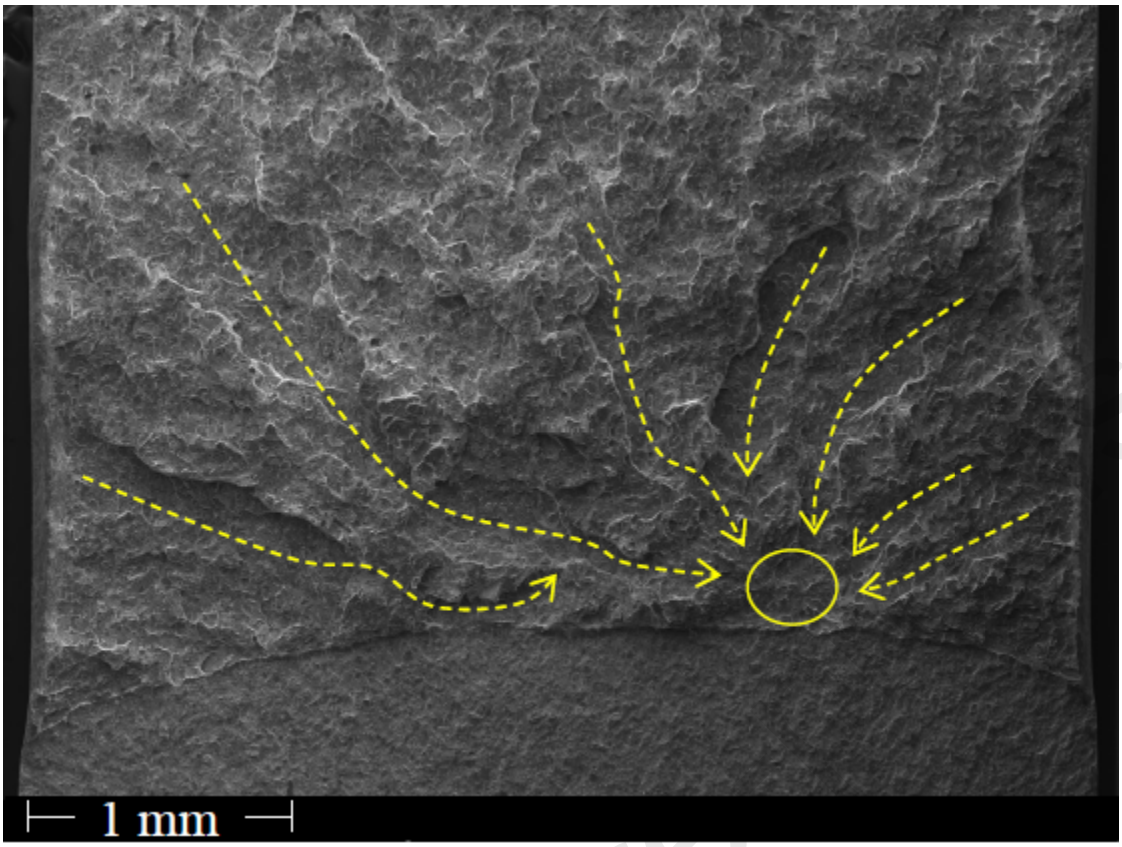
1 mm

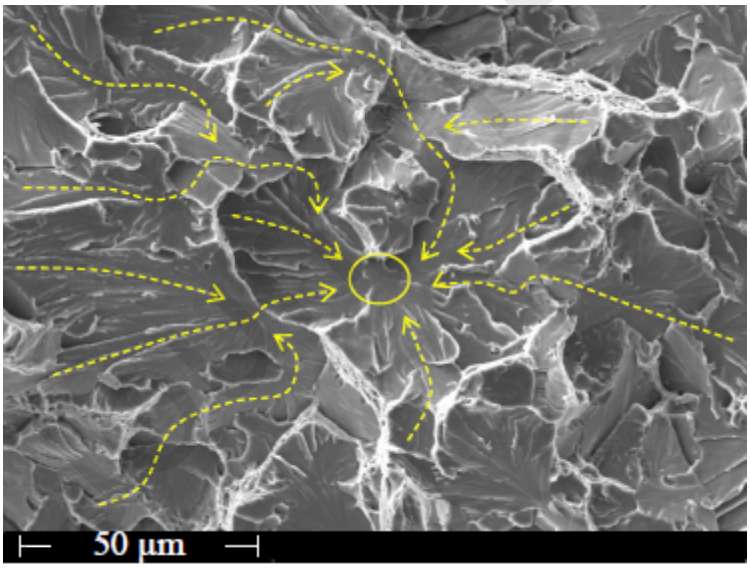
50 µm

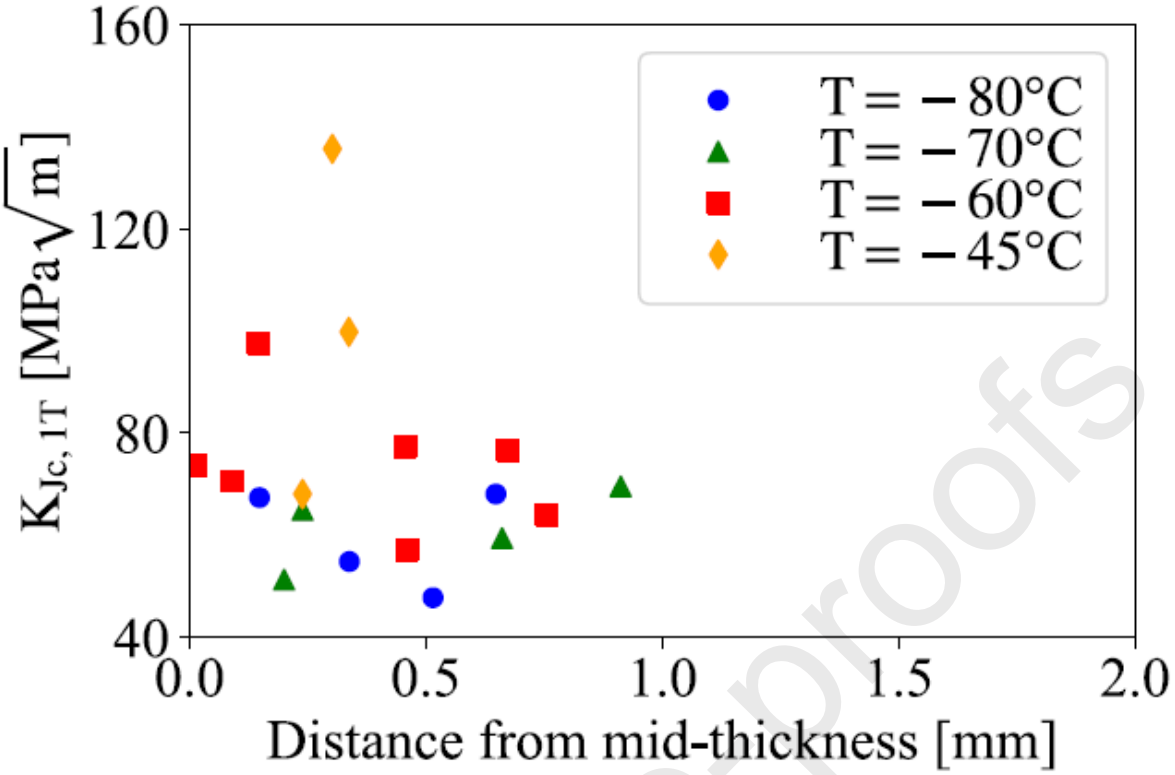

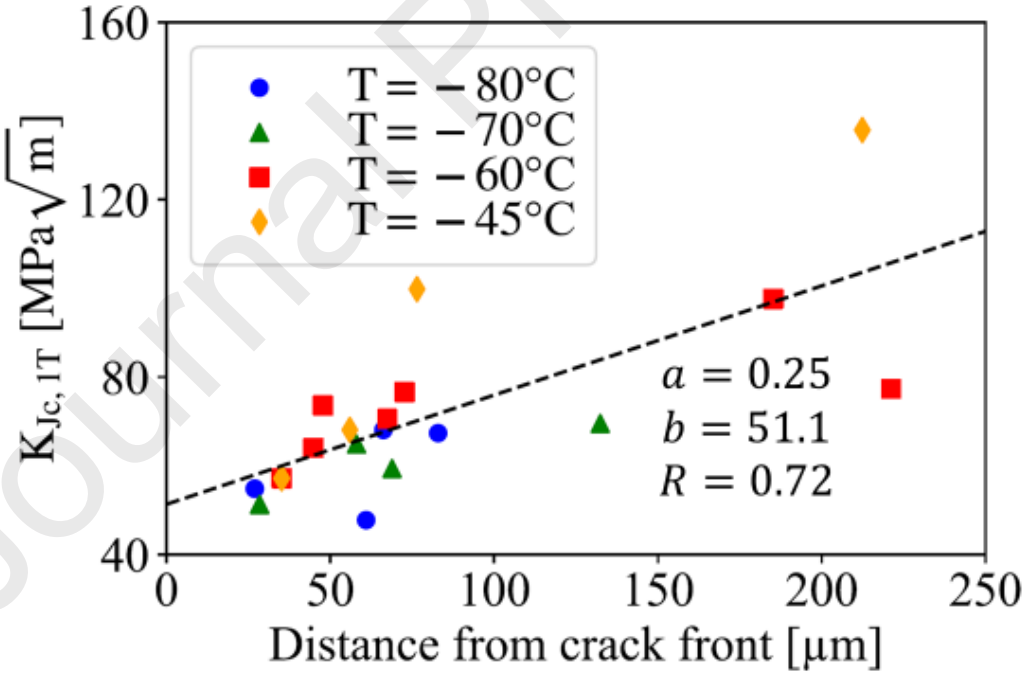

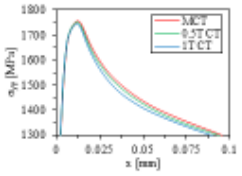

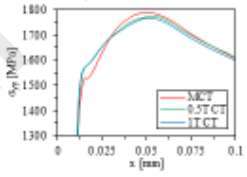

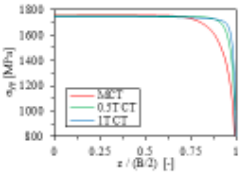

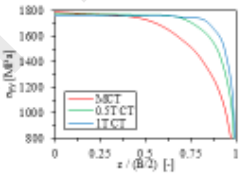

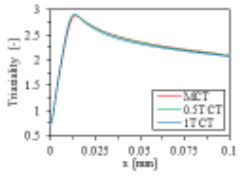

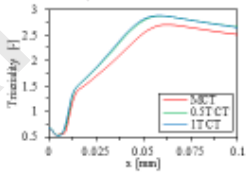

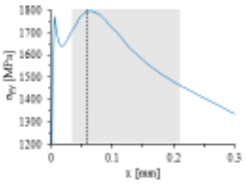

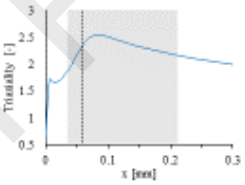

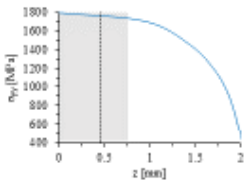

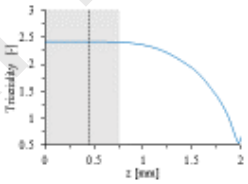

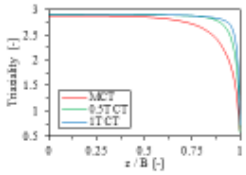

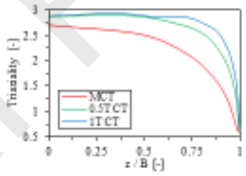

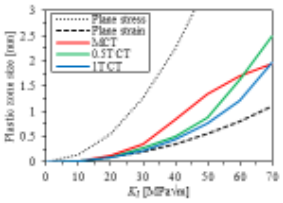

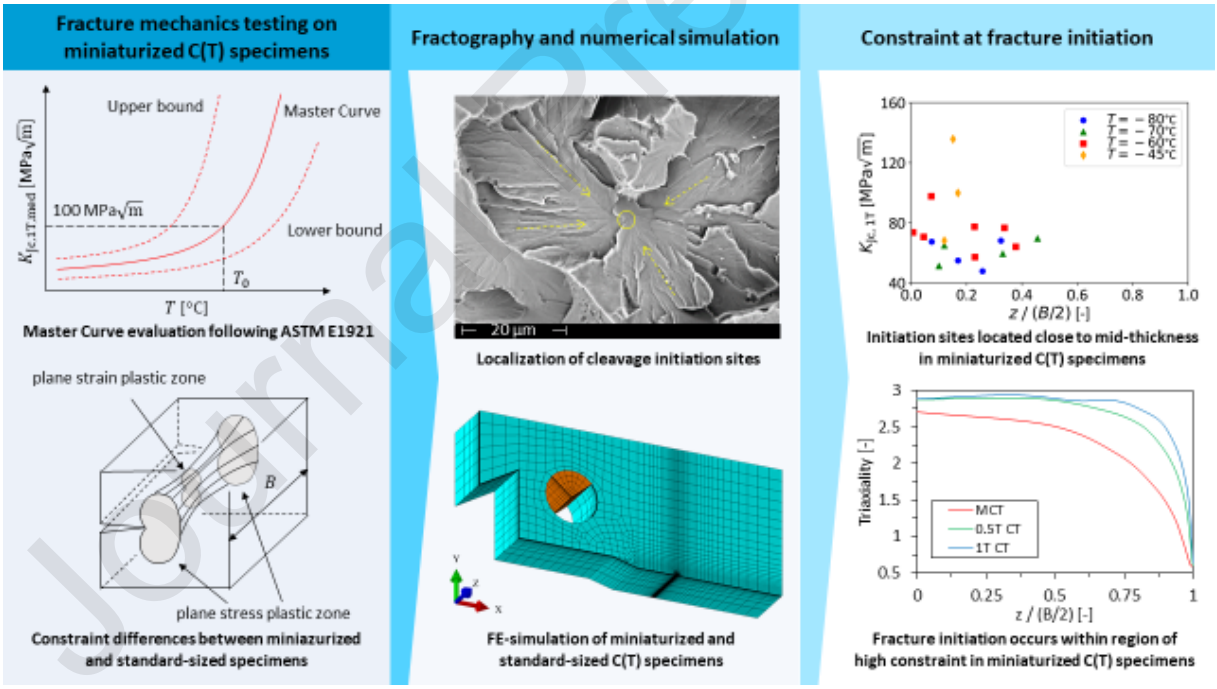

- Cleavage fracture initiation sites of MCT and standard-sized CT specimens are located around mid-thickness
- Significant loss of constraint near side surfaces of MCT specimens is observed as fracture load is approached
- Initiation site locations are aligned with region of high constraint where saturation of triaxiality is observed
- Fracture behavior of MCT specimens is comparable to standard-sized specimens

Declaration of interests

☐ The authors declare that they have no known competing financial interests or personal relationships that could have appeared to influence the work reported in this paper.

☒ The authors declare the following financial interests/personal relationships which may be considered as potential competing interests:

Timo Metzler reports financial support was provided by Euratom Research and Training Programme. If there are other authors, they declare that they have no known competing financial interests or personal relationships that could have appeared to influence the work reported in this paper.